Supporting Information:

Pseudorotaxanes based on tetraazamacrocyclic copper complexes and dibenzocrown ethers

Joanna Małecka[a], Iwona Mames[b], Mateusz Woźny[b], Bohdan Korybut-Daszkiewicz[b], Renata Bilewicz[a]

Table 1S. Voltammetric characteristics of copper(II)/copper(III) and copper(II)/copper(I) processes (CV):

Process	copper(II)/copper(III)					copper(II)/ copper(I)				
Complex	E_{pa1} [V]	E_{pc1} [V]	E_{pa}-$E_{pa/2}$ [mV]	E_{pc}-$E_{pc/2}$ [mV]	$E^{0'}$ [V]	E_{pa1} [V]	E_{pc1} [V]	E_{pa}-$E_{pa/2}$ [mV]	E_{pc}-$E_{pc/2}$ [mV]	$E^{0'}$ [V]
14Cu-Bu	1.015	0.946	59	57	0.934	-0.966	-1.079	67	62	-1.023
14Cu-Bu$_2$	0.945	0.872	61	56	0.931	-1.157	-1.231	58	59	-1.194
14Cu-SS	1.042	0.964	62	60	1.003	-	-1.765	-	75	-

Epa [V] –oxidation peak potential; Epc [V] – reduction peak potential $E^{0'}$ [V] – formal potential;

Table 2S. Redox properties of investigated complexes (DPV):

	copper(II)/copper(III)		copper(II)/ copper(I)	
Complex	E_{pa1} [V]	$b_{1/2}$ [mV]	E_{pa1} [V]	$b_{1/2}$ [mV]
14Cu-Bu	0.979	98	-1.024	99
14Cu-Bu$_2$	0.939	107	-1.192	110
14Cu-SS	0.977	109	-	-

Ep_{DPV} [V] – peak potential; $w_{1/2}$ [mV] – width of the peak at half height

Table 3S. Redox properties of investigated complexes (DPV) in the presence of crown ether:

Complex	$E_{p\ DPV}$ [V]	$w_{1/2}$ [mV]
1Cu-Bu	0.979	98
14Cu-Bu with DB24C8 (1:20)	0.959	98
14Cu-Bu with DB24C8 (1:50)	0.940	100
14Cu-Bu with DB24C8 (1:75)	0.923	99
14Cu-Bu with DB24C8 (1:100)	0.891	103

14Cu-Bu with DB30C10 (1:22)	0.981	98
14Cu-Bu with DB30C10 (1:35)	0.974	98
14Cu-Bu with DB30C10 (1:50)	0.971	107
14Cu-Bu with DB30C10 (1:75)	0.969	117
14Cu-Bu with DB30C10 (1:100)	0.958	122
1Cu-Bu_2	0.939	107
14Cu-Bu_2 with DB30C10 (1:20)	0.930	108
14Cu-Bu_2 with DB30C10 (1:50)	0.921	107
14Cu-Bu_2 with DB30C10 (1:75)	0.915	110
14Cu-Bu_2 with DB30C10 (1:100)	0.906	112
1Cu-SS	1.019	103
14Cu-SS with DB24C8 (1:20)	1.015	102
14Cu-SS with DB24C8 (1:50)	1.002	105
14Cu-SS with DB24C8 (1:75)	0.982	107
14Cu-SS with DB24C8 (1:100)	0.980	107
14Cu-SS with DB30C10 (1:25)	1.013	93
14Cu-SS with DB30C10 (1:35)	1.011	98
14Cu-SS with DB30C10 (1:50)	1.003	107
14Cu-SS with DB30C10 (1:74)	0.998	122
14Cu-SS with DB30C10 (1:100)	0.981	146

Ep_{DPV} [V] – peak potential; $w_{1/2}$ [mV] – width of the peak at half height

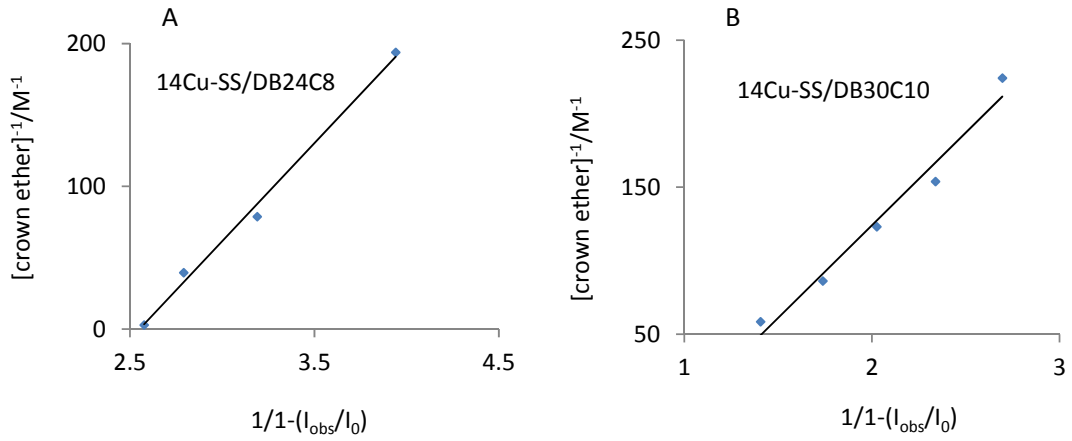

Figure 1S. Plot of 1/[crown ether] versus 1/1-(I_{obs}-I_0) for **14Cu-SS** with DB24C8 (A) and DB30C10 (B).

Kinetics of electrode processes

The scan rate corresponding to the intersection point of the two asymptotes, v_a=v_c is calculated as shown in the plots of Figure 3S. The transfer coefficients (α_{ox} and α_{red}) were obtained by measuring the change of the peak potential with scan rate. A plot of E_p vs. log v yields two straight lines with slopes equal to $2.3RT/\alpha nF$ and $2.3RT/(1-\alpha)nF$ for the anodic and cathodic branches, to give values of α_{ox} = 0,17 and α_{red} = 0,82, and of α_{ox} = 0,46 and α_{red} = 0,66, for the gold electrode covered with mixed monolayer **C_6SH/14Cu-SS** in the supporting electrolyte not containing, and containing 1mM **DB30C10**, respectively.

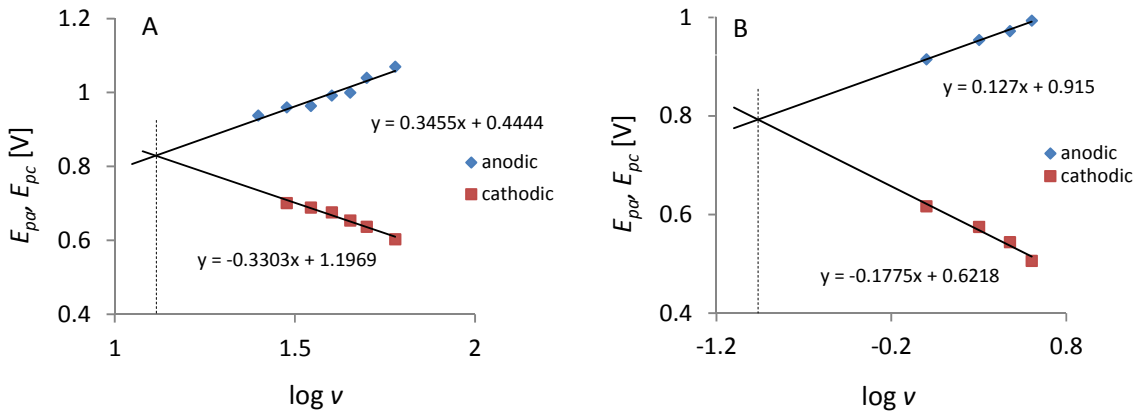

Figure 2S. Voltammetric peak potential versus scan rate dependencies for the gold electrode covered with mixed monolayer **C_6SH/14Cu-SS** in the supporting electrolyte (A) without, and (B) containing 1mM **DB30C10**

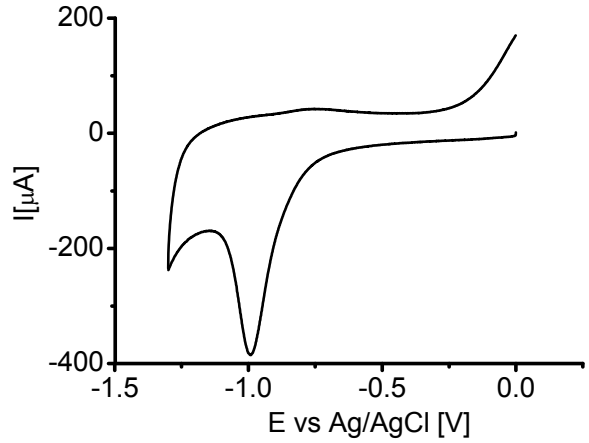

Figure 3S. Electrochemical reductive desorption of a **14Cu-SS** SAM from gold in 0.5M KOH at 100mVs^{-1}.

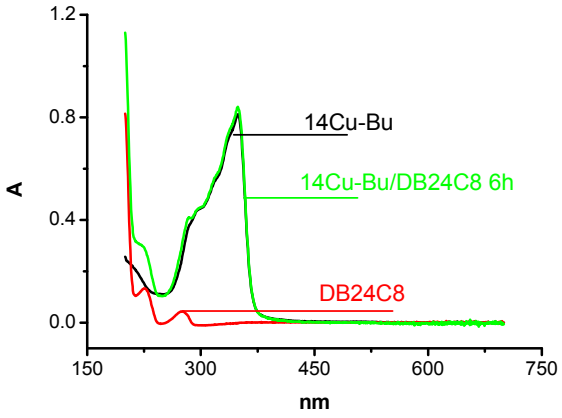

Figure 4S. UV-vis spectra of 14Cu-Bu ($1 \cdot 10^{-5}$ moldm^{-3}) and DB24C8, separately and 6h after mixing.

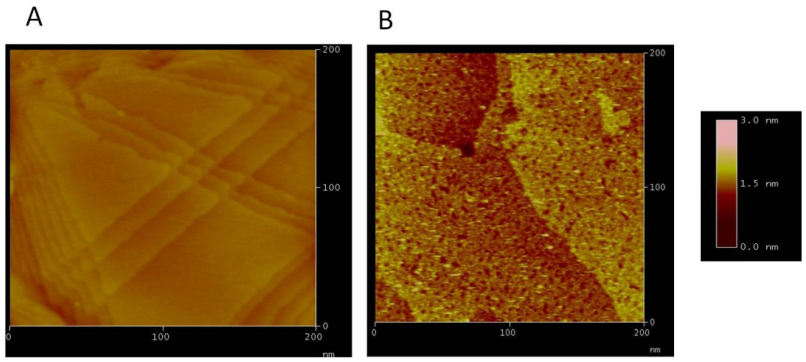

Figure 5S. STM images of surface of bare gold substrate (A); 14Cu-SS monolayer adsorbed on the gold electrode (B).